Continental pollution in the Western Mediterranean basin: large variability of the aerosol single scattering albedo and influence on the direct shortwave radiative effect

Claudia Di Biagio, Paola Formenti, Lionel Doppler, Cécile Gaimoz, Noël Grand, Gérard Ancellet, Jean-Luc Attié, S. Bucci, Philippe Dubuisson, Federico Fierli, et al.

Atmos. Chem. Phys. Discuss., doi:10.5194/acp-2016-47, 2016
Manuscript under review for journal Atmos. Chem. Phys.
Published: 11 April 2016

Atmospheric Chemistry and Physics Discussions

Continental pollution in the Western Mediterranean basin: large variability of the aerosol single scattering albedo and influence on the direct shortwave radiative effect

C. Di Biagio[1], P. Formenti[1], L. Doppler[2], C. Gaimoz[1], N. Grand[1], G. Ancellet[3], J.-L. Attié[4,5], S. Bucci[6,7], P. Dubuisson[8], F. Fierli[6], M. Mallet[9], and F. Ravetta[3]

[1] *LISA, UMR CNRS 7583, Université Paris Est Créteil et Université Paris Diderot, Institut Pierre Simon Laplace, Créteil, France*

[2] *Deutscher Wetterdienst, Metorological Observatory Lindenberg, Germany*

[3] *Sorbonne Universités, UPMC Univ. Paris 06; Université Versailles St-Quentin; CNRS/INSU, LATMOS-IPSL, Paris, France*

[4] *Laboratoire d'Aérologie, University of Toulouse, UMR 5560 CNRS, France*

[5] *CNRM GAME UMR 3589 CNRS, METEO-FRANCE*

[6] *Institute for Atmospheric Sciences and Climate of the National Research Council , (ISAC-CNR), Rome, 00133, Italy*

[7] *Sc. Dept. of Physics, Ferrara University, Ferrara, 44121, Italy*

[8] *Laboratoire d'Optique Atmosphérique, Université Lille 1, Villeneuve d'Ascq, France*

[9] *Laboratoire d'Aérologie, Observatoire Midi-Pyrénées, 14 Avenue Edouard Belin, 31400 Toulouse, France*

Corresponidng author:

Claudia Di Biagio, claudia.dibiagio@lisa.u-pec.fr

Atmos. Chem. Phys. Discuss., doi:10.5194/acp-2016-47, 2016
Manuscript under review for journal Atmos. Chem. Phys.
Published: 11 April 2016

Atmospheric Chemistry and Physics Discussions

Abstract

Pollution aerosols strongly influence the composition of the Western Mediterranean basin, but at present little is known on their optical properties. We report in this study in situ observations of the single scattering albedo (ω) of pollution aerosol plumes measured over the Western Mediterranean basin during the TRAQA (TRansport and Air QuAlity) airborne campaign in summer 2012. Cases of pollution export from different source regions around the basin and at different altitudes between ~160 and 3500 m above sea level have been sampled during the flights. Data from this study show a large variability of ω, with values between 0.84-0.98 at 370 nm and 0.70-0.99 at 950 nm. The single scattering albedo generally decreases with the wavelength, with some exception associated to the mixing of pollution with sea spray over the sea surface. Lowest values of ω (0.84-0.70 between 370 and 950 nm) are measured in correspondence of a fresh plume possibly linked to ship emissions over the basin. The range of variability of ω observed in this study seems to be independent of the source region around the basin, as well as of the altitude and ageing time of the plumes. The observed variability of ω reflects in a large variability for the complex refractive index of pollution aerosols, which is estimated to span in the large range 1.41-1.75 and 0.002-0.068 for the real and the imaginary parts, respectively, between 370 and 950 nm.

Radiative calculations in clear-sky conditions have been performed with the GAME radiative transfer model to test the sensitivity of the aerosol shortwave Direct Radiative Effect (DRE) to the variability of ω as observed in this study. Results from the calculations suggest up to a 50% and 30% change of the forcing efficiency (FE), i.e. the DRE per unit of optical depth, at the surface (-160÷-235 $Wm^{-2}\tau^{-1}$ at 60° solar zenith angle) and at the Top-Of-Atmosphere (-137÷-92 $Wm^{-2}\tau^{-1}$) for ω varying between its maximum and minimum value. This induces a change of up to an order of magnitude (+23÷+143 $Wm^{-2}\tau^{-1}$) for the radiative effect within the atmosphere.

Keywords: pollution aerosols, single scattering albedo, direct radiative effect, Western Mediterranean

Atmos. Chem. Phys. Discuss., doi:10.5194/acp-2016-47, 2016
Manuscript under review for journal Atmos. Chem. Phys.
Published: 11 April 2016

Atmospheric Chemistry and Physics Discussions

1. Introduction

Atmospheric aerosols play a crucial role on climate by affecting the radiative transfer of atmospheric radiation and by modifying cloud properties and lifetime (Boucher et al., 2013). The capability of atmospheric aerosols to interact through processes of scattering and absorption with the atmospheric radiation, so to exert a direct radiative effect (DRE), depends on their spectral optical properties (extinction efficiency, k_{ext}, single scattering albedo, ω, and asymmetry factor, g). In particular the single scattering albedo has been demonstrated to be a key parameter in modulating the surface, Top-of-Atmosphere (TOA), and atmospheric aerosol DRE (e.g., Ramana and Ramanathan, 2006; Di Biagio et al., 2010; Loeb and Su, 2010). Aerosol optical properties can largely vary depending on the particles composition, size distribution, and shape, which are function of the aerosol source, type, and processing occurring during atmospheric lifetime. At present, the capability of climate models in reproducing all the possible heterogeneity in aerosol optical properties represents one the main source of uncertainty in evaluating their DRE on climate (McComiskey et al., 2008; Stier et al., 2013). In this sense, intensive studies providing with the characterization of the aerosol optical properties and their local and regional variability are of great importance in order to reduce these uncertainties.

This is particularly the case of the Western Mediterranean basin. Indeed, the Mediterranean is a very complex region, characterized by the presence of air masses carrying aerosols of different origins and types (Gkikas et al., 2012). On its northern bound, it is limited by Europe, which makes that anthropogenic pollution is usually exported from the continent towards the basin (Lelieveld et al., 2002; Pace et al., 2006). In particular, the Western part of the Mediterranean basin, surrounded by large coastal megacities, commercial harbours, and under the direct influence of some of the most industrialized areas of the continent (such as the Po Valley in Northern Italy or the Fos/Berre area in Southern France), is strongly affected by continental pollution outflows (Pérez et al., 2008; Pey et al., 2010; Di Biagio et al., 2015). The build-up of high pollution levels over the Western basin is particularly favoured during summer when the strong insolation enhances photochemical reactions and the stable meteorological conditions promote the stagnation of pollutants (Millan et al., 2000; Mallet et al., 2005).

In spite of this, the characterization of the optical properties of anthropogenic aerosols in this part of the basin remains only limited to coastal and inland regions (Mallet et al., 2003, 2011, 2013; Lyamani et al., 2006; Estelles et al., 2007; Saha et al., 2008; Esteve et al., 2012;

Atmos. Chem. Phys. Discuss., doi:10.5194/acp-2016-47, 2016
Manuscript under review for journal Atmos. Chem. Phys.
Published: 11 April 2016

Atmospheric Chemistry and Physics Discussions

Piazzola et al., 2012; Pandolfi et al., 2011 and 2014), or remote islands actually far from the strong influence of continental outflows (Lyamani et al., 2015). Moreover, the majority of these studies uses remote sensing measurements and analyse aerosol properties integrated over the entire atmospheric column, without information on their vertical variability. Thus, at present, we miss a detailed characterization of the optical properties of the pollution aerosol over the entire region, in particular over the remote sea, and its vertical distribution.

To fill this gap, the international ChArMEx (Chemistry-Aerosol Mediterranean Experiment; http://charmex.lsce.ipsl.fr) research program has supported in recent years two airborne campaigns over the Western Mediterranean basin: TRAQA (Transport and Air QuAlity) in 2012 and SAFMED (Secondary Aerosol Formation in the MEDiterranean) in 2013.

In a recent paper, Di Biagio et al. (2015) have presented in situ measurements of the aerosol vertical profiles acquired over the remote sea during these campaigns. Observations from TRAQA and SAFMED have shown that in the Western basin pollution plumes extend as far as hundreds of km from the coastline and reach up to ~4000 m, presenting a complex stratified structure, and pollution plumes show a large heterogeneity in terms of composition, origin, and lifetime.

Following these observations, we may ask: does the heterogeneity in pollution plume composition, origin, and lifetime as observed in Di Biagio et al. (2015) induce heterogeneity on the optical properties (in particular the single scattering albedo) of pollution aerosols in this part of the basin? And, if observed, does this heterogeneity on the optical properties influence the aerosol DRE? Is it necessary to take it into account to better evaluate the aerosol radiative impact in the Western Mediterranean?

With the aim of answering these questions, in this paper we analyse data of the optical properties (spectral scattering and absorption coefficients, and single scattering albedo) and size distributions of pollution aerosols measured over the Western Mediterranean basin during TRAQA. SAFMED observations have been excluded here given that only limited data on the aerosol optical properties are available from this campaign. The objective of the paper is twofold: to provide a new dataset of aerosol single scattering albedo values which can be representative of the polluted aerosols over the Western basin, and investigate the sensitivity of the aerosol direct DRE to the variability of this parameter.

Atmos. Chem. Phys. Discuss., doi:10.5194/acp-2016-47, 2016
Manuscript under review for journal Atmos. Chem. Phys.
Published: 11 April 2016

Atmospheric Chemistry and Physics Discussions

2. Overview of flights during the TRAQA campaign

The TRAQA campaign took place in the period 20 June – 13 July 2012. Instruments were installed on board the SAFIRE (Service des Avions Français Instruments pour la Recherche en Environnement, http://www.safire.fr/) tropospheric aircraft ATR-42, based in Toulouse (43° 36' N, 1° 26' E, France). A total of seventeen flights, most often two flights per day, with intermediate stops in different airports in southern France and Corsica, were performed (flight numbers V16 to V32). The majority of flights were over the sea, with some exceptions investigating inland areas in southern France. The flight altitude for the ATR-42 ranged between a minimum of ~60 m to a maximum of ~5000 m above sea level (a.s.l.), and the maximum flight time was 4 h. The general flight strategy consisted of legs at constant altitude to sound the vertical structure by lidar observations, vertical ascents/descents to describe the vertical atmospheric column and identify the main aerosol plumes, followed by straight levelled runs (SLRs) within the detected aerosol layers. In the present study we will exclusively consider measurements acquired during SLRs, since only during these phases the whole set of aerosol optical properties (scattering and absorption coefficients) were measured. A total of 21 SLRs were performed over the sea surface or inland close to the coastline and will be considered in this study. Figure 1 and Table 1 summarise the geographical location, time, and altitude of these 21 SLRs. As indicated in Table 1 each SLR was about 15-20 min long. At the cruise speed of the ATR (93 ms^{-1}), this integration time corresponds to about 100 km.

3. Measurements and methods

3.1 Aircraft observations

Aerosol sampling on the ATR-42 was performed using the AVIRAD system. AVIRAD is an iso-axial and iso-kinetic inlet which samples air at a volumetric flow of ~350 L min^{-1}. The 50% passing efficiency of the inlet is 12 µm diameter. Various lines depart from AVIRAD to connect to different instruments for the measurement of the aerosol physico-chemical and optical properties. Additionally, several sensors for the measurements of the atmospheric composition were installed on the ATR-42 aircraft as basic equipment. A brief description of the different in situ measurements considered in this study from the AVIRAD system and the ATR-42 equipment and their data analysis is reported in the following.

- The aerosol scattering coefficient (σ_s) at 450, 550, and 700 nm has been measured by a 3-wavelengths integrating nephelometer (TSI Inc., model 3563, 6s resolution). The

Atmos. Chem. Phys. Discuss., doi:10.5194/acp-2016-47, 2016
Manuscript under review for journal Atmos. Chem. Phys.
Published: 11 April 2016

Atmospheric Chemistry and Physics Discussions

nephelometer was calibrated prior the campaign by using air and CO_2 as reference gases. Nephelometer measurements have been corrected for angular truncation and Lambertian non-idealities by applying the formula by Anderson and Ogren (1998), appropriated to submicron aerosols which we expected in the pollution plumes sampled during the campaign. The measurement uncertainty on σ_s, calculated taking into account for the photon counting, gas calibration, and angular corrections uncertainties, is estimated to be lower than 10% at the three wavelengths. Averages of the scattering coefficient are calculated over the different SLRs. The uncertainty on the SLR average values is estimated as the combination of the measurement uncertainty and the standard deviation along each individual run. For each SLR, the particle scattering Ångström exponent (SAE) has been calculated as the power law fit of the measured scattering coefficients versus wavelength to extrapolate the scattering coefficient at other wavelengths than those of operation.

The nephelometer measured the scattering coefficient in dry air conditions. This is due to the heating of the airflow while entering the aircraft cabin and the temperature increase in the sensing volume of the instrument due to illumination. The relative humidity measured during the flights inside the nephelometer cavity was <25% in more than 90% of cases, with values up to ~40% occasionally observed <200 m over the sea surface.

- The aerosol absorption coefficient (σ_{abs}) at 370, 470, 520, 590, 660, 880, and 950 nm has been measured by a 7-wavelengths aethalometer (Magee Sci., model AE31, 2min resolution). The principle of operation of the aethalometer consists in measuring the attenuation of light through an aerosol-laden filter compared to that of another portion of the filter which is unexposed to the air flow and is used as a reference (Weingartner et al., 2003). To yield the aerosol absorption coefficient, the spectral attenuation $\sigma_{ATT}(\lambda)$ measured by the aethalometer has been corrected following the procedure described by Collaud Coen et al. (2010):

$$\sigma_{abs}(\lambda) = \frac{\sigma_{ATT}(\lambda) - \alpha(\lambda)\overline{\sigma_s(\lambda)}}{C_{ref} R(\lambda)} \qquad (1).$$

The different terms in equation 1 are: (i) $\alpha(\lambda)\overline{\sigma_s(\lambda)}$ or "scattering correction". In this work $\alpha(\lambda)$ has been calculated with the formula by Arnott et al. (2005) and varies between 0.02 and 0.07, while $\overline{\sigma_s(\lambda)}$ is the average of the scattering coefficient along the considered SLR extrapolated at the aethalometer wavelengths; (ii) C_{ref} or "multiple scattering correction".

Atmos. Chem. Phys. Discuss., doi:10.5194/acp-2016-47, 2016
Manuscript under review for journal Atmos. Chem. Phys.
Published: 11 April 2016

Atmospheric Chemistry and Physics Discussions

C_{ref} is set to 2.14 ± 0.21 (wavelength-independent) following Weingartner et al. (2003); (iii) $R(\lambda)$ or "shadowing effect correction". $R(\lambda)$ depends on the charge and absorptivity properties of the sampled aerosol and can be calculated as a function of the particle single scattering albedo (ω). In this study, because of the absence of an independent determination of ω, we used an estimated "first-guess" single scattering albedo (ω^*) to calculate R. This has been determined as the ratio of the measured scattering (σ_s) to extinction ($\sigma_s + \sigma^*_{abs}$) coefficients, with σ^*_{abs} corrected for the scattering and the multiple scattering corrections, but not for the shadowing effect. The obtained $R(\lambda)$ varies between 0.75 and 1 for ω^* between 0.75-0.99 at 370 nm and 0.70-0.99 at 950 nm. The whole uncertainty on the absorption coefficient has been estimated with the propagation error formula taking into account for the different factors in Eq. (1) and varies between 11-36% at 370 nm and 12-70% at 950 nm.

It has to be noticed that an enhanced absorption at single wavelengths has been observed in several cases for the aethalometer. This is possibly due to the absorption on the exposed filter of gases or volatile compounds absorbing at some of the instrument operating wavelengths (Weingartner et al., 2003). These anomalous points have been accurately selected and screened from the dataset. As a result of this screening, data in correspondence of only 60% of the considered SLRs are available for aerosols analyses.

The measured aerosol scattering and absorption coefficients have been used to calculate the particle spectral single scattering albedo (ω) between 370 and 950 nm as:

$$\omega(\lambda) = \frac{\sigma_s(\lambda)}{\sigma_s(\lambda) + \sigma_{abs}(\lambda)} \qquad (2).$$

The uncertainty on ω has been calculated with the propagation error formula and varies between 0.02 and 0.04 at all wavelengths.

Additionally, for each SLR for which aethalometer data are available, the particle absorption Ångström exponent (AAE) has been calculated as the power law fit of the measured absorption coefficients versus wavelength.

- The aerosol number size distribution ($dN/dlogD_g$) has been measured by two different optical particle spectrometers: the passive cavity aerosol spectrometer probe (PCASP, model 100-X, 1-s resolution, 31 size classes between 0.1 and 3.0 µm diameter, operating wavelength 632.8 nm), and the optical particle spectrometer SkyGRIMM (GRIMM Inc., model 1.129, 6-s resolution, 32 size classes between 0.3 and 32 µm diameter, operating

Atmos. Chem. Phys. Discuss., doi:10.5194/acp-2016-47, 2016
Manuscript under review for journal Atmos. Chem. Phys.
Published: 11 April 2016

Atmospheric Chemistry and Physics Discussions

wavelength 655 nm). For both the PCASP and the SkyGRIMM, the measured sphere-equivalent optical diameter has been converted in a sphere-equivalent geometrical diameter (D_g) by taking into account the complex refractive index of the sampled aerosol (Liu and Daum, 2000). Calculation are performed by fixing the imaginary part of the refractive index at 0.01, thus representing a medium absorbing aerosol, while varying the real part between 1.50 and 1.72, following the range of variability found in the literature for pollution aerosols in the Mediterranean (see Di Biagio et al., 2015 for further details). D_g is then set at the mean ± one standard deviation of the values obtained for the different n. After refractive index correction the D_g ranges for the PCASP and the SkyGRIMM become 0.10-4.47 and 0.28-65.80 µm, with an uncertainty between 1 and 25%. The smallest and the largest size bins of both instruments, for which the minimum and maximum edges respectively are not defined, have been excluded from the datasets, thus reducing the PCASP and SkyGRIMM D_g ranges to 0.11-4.17 µm and 0.31-56.21 µm, respectively.

Corrected data from the PCASP and the SkyGRIMM are then merged to obtain the aerosol size distribution over a larger size range. The two instruments superimpose in a large interval covering the diameter range ~0.31-4.17 µm. In this interval the PCASP and the GRIMM show a good agreement below 0.4 µm and above 1.0 µm (less than ~10% difference), while significant differences are observed in the 0.4-1.0 µm range where the PCASP underestimates the SkyGRIMM measurements by more than ~50%. This difference is of great relevance in terms of optical properties because particles in the 0.4-1.0 µm size interval are very efficient for interaction with shortwave radiation. With the aim of understanding which of the two instruments measures correctly in the 0.4-1.0 µm range we have performed an optical test, which consisted in calculating with Mie theory the scattering coefficient at 450, 550, and 700 nm based on the PCASP and SkyGRIMM size data, and then in comparing it with simultaneous nephelometer measurements. Optical calculations have been performed by fixing the complex refractive index at 1.6-0.01i, so at the mean of the range of values reported in the literature for pollution aerosols (Ebert et al., 2002 and 2004; Mallet et al., 2003 and 2011; Müller et al., 2002; Raut and Chazette, 2008). SLRs characterized by a low variability in terms of scattering coefficient and particle concentration have been selected. The results of the optical test indicate that in the 0.4-1.0 µm range the size distribution of the SkyGRIMM is more accurate since it permits to most closely reproduce nephelometer observations (<5% mean difference between

Atmos. Chem. Phys. Discuss., doi:10.5194/acp-2016-47, 2016
Manuscript under review for journal Atmos. Chem. Phys.
Published: 11 April 2016

Atmospheric Chemistry and Physics Discussions

calculations and observations at the three wavelengths, compared to differences up to 15-21% if PCASP data are used in the 0.4-1.0 µm size range). Thus, a combined PCASP-SkyGRIMM number size distribution $dN/dlogD_g$ in the 0.11 to 56.21 µm diameter range has been calculated by considering PCASP data up to 0.31 µm and SkyGRIMM data above. Together with the number size distribution, for each SLR also the volume size distribution $dV/dlogD_g=\pi/6\, D_g^3\, dN/dlogD_g$ has been calculated.

Nonetheless, due to a technical problem, SkyGRIMM data were only available below ~350 m (~970 hPa).

- The total particle number concentrations in the Aitken (4 nm-0.1 µm; dN_{Aitken}) and accumulation (0.1-1.0 µm; dN_{Acc}) modes have been calculated by combining condensation particle counter measurements of particle concentration in the 0.004 – 3 µm range (CPC, TSI Inc., model 3775, 5-s resolution) and size distribution data. Due to the fact that above 350 m the SkyGRIMM is not available, only PCASP data are used in the calculations of dN_{Aitken} and dN_{Acc} over the whole altitude range. dN_{Aitken} is estimated as the difference between CPC concentration and the integral of PCASP data between 0.1 and 3.0 µm, while dN_{Acc} is obtained by integrating the PCASP number concentrations in the 0.1-1.0 µm interval. The underestimation of the PCASP number concentration between 0.4 and 1.0 µm, as discussed above, is estimated to induce a ~20% underestimation of the dN_{Acc} calculated here, whilst it has almost a negligible impact on dN_{Aitken}. The dN_{Acc} and dN_{Aitken} obtained in correspondence of each SLR have been used to calculate the Aitken-to-accumulation ratio dN_{Aitken}/dN_{Acc}.
- The carbon monoxide (CO) and ozone (O_3) mixing ratios have been measured by the MOZART instrument (CO, 30-s resolution and ±5% nominal uncertainty, O_3, 4-s resolution and ±2% nominal uncertainty) (Nedelec et al., 2003). Starting from the measured O_3 and CO, the ozone enhancement ratio ($\Delta O_3/\Delta CO$) has been calculated, i.e. the ratio of the ozone to carbon monoxide variations compared to their baseline values. A background value of ~70 ppbv in the boundary layer and ~60 ppbv in the free troposphere has been used for CO, while the background has been set at ~30 ppbv for O_3 at all levels (Di Biagio et al., 2015). $\Delta O_3/\Delta CO$ data have been used together with dN_{Aitken}/dN_{Acc} to retrieve information on the age of the sampled air masses, as discussed in Di Biagio et al. (2015).

In order to compare SLRs measurements obtained at different altitudes, the data analysed here are reported to standard temperature and pressure (STP) using T=293.15 K and

Atmos. Chem. Phys. Discuss., doi:10.5194/acp-2016-47, 2016
Manuscript under review for journal Atmos. Chem. Phys.
Published: 11 April 2016

Atmospheric Chemistry and Physics Discussions

P=1013.25 hPa. In this case, the scattering and absorption coefficients are scaled to STP conditions and the particle concentrations (in number or volume) are given as particles per standard cm^{-3} (scm^{-3}). Where not explicitly indicated, data refer to STP conditions.

In Table 2 we summarize main information and uncertainties for the different aerosol instruments considered in this study.

3.2 Boundary layer height estimation

The planetary boundary layer (BL) top height has been estimated from meteorological observations (temperature, T, potential temperature, θ, and relative humidity, RH) for each vertical sounding performed during TRAQA flights (see Di Biagio et al., 2015). The boundary layer top height is between 730 and 1500 m, with an average of ~1000 m. The location of each SLR, so if it is within the boundary layer or in the free troposphere, has been determined based on the planetary boundary layer top height estimated from the closest vertical sounding performed during each flight.

3.3 Tracking the origin of the sampled air masses

As discussed in Di Biagio et al. (2015), aerosol observations during TRAQA were mostly influenced by pollution/anthropogenic particles exported from different sources around the basin (Northern Italy/Po Valley, Southern France, Barcelona area). The Lagrangian trajectory model FLEXPART (FLEXible PARTicle dispersion model, Stohl et al., 1998), adapted for the WRF (Weather Research and Forecasting) meteorological input (Brioude et al., 2013) has been used here to track the origin of air masses sampled during SLRs. Five-day three-dimensional back-trajectories have been calculated using the WRF meteorological output at a 30 km horizontal resolution and 28 vertical model levels up to 50 hPa. The model specific humidity and potential vorticity is also interpolated along the trajectory path. Based on FLEXPART simulations, data for the different SLRs have been separated as a function of the origin of the sampled air masses. Three different sectors have been defined: the Western sector, which includes trajectories coming from the Atlantic Ocean and travelling over France or northern Spain before reaching the Western basin; the Eastern sector, including air mass trajectories from continental Europe that have travelled over northern Italy-Po Valley before entering the basin; and the Open Sea sector, which consists of trajectories coming from the Western or Eastern sectors which have experienced at least 2 days of subsidence over the sea in the Western basin and thus can be taken as representative of the regional background

Atmos. Chem. Phys. Discuss., doi:10.5194/acp-2016-47, 2016
Manuscript under review for journal Atmos. Chem. Phys.
Published: 11 April 2016

Atmospheric Chemistry and Physics Discussions

aerosol or local pollution sources, i.e. ship emissions. The three different selected Sectors are shown in Fig. 1, while Table 1 also reports the identified Sector of origin for the air masses sampled during the different SLRs. As discussed in Di Biagio et al. (2015), several flights were affected by dust particles exported over the basin from Northern Africa. SLRs data dominated by dust have been identified based on the combined analysis of back-trajectories, lidar profiles and optical data, and have been excluded from the dataset. However, for some SLRs, the possible mixing of dust aerosols with pollution particles cannot be a priori excluded.

3.4 Radiative model calculations

Radiative transfer calculations have been performed to estimate the instantaneous aerosol direct radiative effect in the shortwave spectral range for different cases and in clear-sky conditions. The objective of the calculations is to test the sensitivity of the DRE to the variability of the aerosol optical properties, in particular the single scattering albedo, as observed in this study. The GAME radiative transfer model (Dubuisson et al., 1996 and 2006) has been used in this study to compute the vertical profiles of downward and upward shortwave irradiances over the 0.28-3.0 µm spectral range. The model calculates radiances and irradiances at various atmospheric levels at 400 cm^{-1} spectral resolution between 0.28 and 0.5 µm and 100 cm^{-1} resolution between 0.5 and 3 µm. Spectral absorption by principal atmospheric gases (H_2O, CO_2, O_3, CH_4, N_2O, O_2) is taken into account in the model. The discrete ordinate method (Stamnes et al., 1988) with twelve streams is used in the simulations to describe multiple scattering. Simulations have been performed with and without aerosols by fixing the solar zenith angle (θ) at 60°, i.e. at about the mean of the diurnal value at the latitudes of north-Western Mediterranean, and for a mid-latitude climatological summer meteorological profile. The aerosol optical properties that are used as input in the GAME radiative code are the spectral variation of the optical depth (τ), the asymmetry parameter (g) and the single scattering albedo (ω). The difference of the net shortwave fluxes (downward minus upward irradiances) with and without aerosols at the surface and at TOA is used to estimate the aerosol DRE at these two levels. The atmospheric DRE is then calculated as the difference between the TOA and the surface values. Finally, the ratio of the DRE to the aerosol optical depth at 500 nm, i.e. the aerosol forcing efficiency (FE), is obtained. The shortwave heating rate at the altitude z is also calculated as:

Atmos. Chem. Phys. Discuss., doi:10.5194/acp-2016-47, 2016
Manuscript under review for journal Atmos. Chem. Phys.
Published: 11 April 2016

Atmospheric Chemistry and Physics Discussions

$$\frac{\partial T}{\partial t} = -\frac{1}{\rho C_p}\frac{\partial F(z)}{\partial z} \quad (3)$$

where T is the air temperature, ρ is the air density, C_p is the specific heat of the air, and F(z) is the net flux at the altitude z.

4. Results

4.1 Overview over the different SLRs

Figure 2 shows the averages altitude, spectral scattering (σ_s) and absorption (σ_{abs}) coefficients, scattering and absorption Ångström exponent (SAE and AAE, respectively), ozone enhancement factor ($\Delta O_3/\Delta CO$), and Aitken-to-accumulation ratio (dN_{Aitken}/dN_{Acc}) measured for the different SLRs during TRAQA.

As shown in Fig. 2 and Table 1, the large majority of the SLRs were performed within the boundary layer at an altitude <1000 m. Only four SLRs (V25_R2, V25_R3, V26_R1, and V30_R1) measured aerosols in the free troposphere between 1800 and 3500 m. The sampled aerosols originated in each of the three different source sectors identified based on FLEXPART back-trajectories (Western, Easter, and Open Sea), with a larger number of cases from the Western sector compared to the Eastern and the Open Sea areas.

For all the different cases, the measured scattering coefficient is in the range 16-73 Mm^{-1} at 450 nm and 8-30 Mm^{-1} at 700 nm. The absorption coefficient is generally below 10 Mm^{-1} at all wavelengths, with the exception of V27_R1 and V32_R1 for which values up to ~20 Mm^{-1} at 370 nm have been measured. For these two cases also the highest values of the particle concentration in the accumulation mode (~1700-2200 # cm^{-3}, not shown) and among the highest values of the scattering coefficient are measured. For all cases, both σ_s and σ_{abs} decrease with the wavelength. The pronounced spectral variability of σ_s, in particular, indicates the dominance of pollution/anthropogenic fine particles in the sampled plumes.

The SAE varies between 0.96 and 1.94, while the AAE varies between 0.92 and 1.65, with an average of ~1.20. The AAE has been not calculated for few cases with very low values of the absorption coefficient (σ_{abs} at 370 nm < 1.5 Mm^{-1}). Both the SAE and the AAE obtained in this study fall in the range of variability indicated by several authors to identify pollution/anthropogenic aerosols or pollution mixed with other aerosol types in the Mediterranean basin (SAE>1-1.5, and AAE~1-1.5; Pace et al., 2006; Toledano et al., 2007; Mallet et al., 2013). Values of AAE larger than unity, in particular, might suggest the possible

Atmos. Chem. Phys. Discuss., doi:10.5194/acp-2016-47, 2016
Manuscript under review for journal Atmos. Chem. Phys.
Published: 11 April 2016

Atmospheric Chemistry and Physics Discussions

389 mixing of pollution with brown carbon or dust particles over the basin (Russell et al., 2010;
390 Mallet et al., 2013).

391 For all the measured SLRs the $\Delta O_3/\Delta CO$ and the dN_{Aitken}/dN_{Acc} ratios vary in the range 0.37-
392 1.02 and 1-50, respectively, for O_3 and CO varying between 24-78 and 69-136 ppbv and
393 dN_{Aitken} and dN_{Acc} between 320-22500 and 100-2170 # cm^{-3}. $\Delta O_3/\Delta CO$ and the dN_{Aitken}/dN_{Acc}
394 are linked to the photochemical (rate of ozone formation) and physical (rate of Aitken to
395 accumulation particle conversion) processes responsible for the ageing of the aerosol plumes.
396 The range of measured values here includes both cases with high dN_{Aitken}/dN_{Acc} and low
397 $\Delta O_3/\Delta CO$, typical of fresh plumes, and cases with low dN_{Aitken}/dN_{Acc} and high $\Delta O_3/\Delta CO$,
398 indicative of more aged air masses (Di Biagio et al., 2015).

399 The summary of these observations suggests that the set of SLRs measurements considered in
400 this study can be considered representative of a wide range of different atmospheric
401 conditions occurring over the basin both in terms of sources, loadings, and lifetime for
402 pollution aerosols.

403

404 **4.2 Particle size distributions**

405 Figure 3 shows the mean and the range of variability of the number and volume size
406 distributions measured during horizontal SLRs within pollution layers during TRAQA. Data
407 refers only to cases at <350 m altitude within the boundary layer. The absolute uncertainty on
408 the measured concentration, as also reported in Table 2, is ~15% for particle diameters below
409 0.31 μm and ~10% at larger sizes. The grey shading indicates considerable variability in the
410 number concentration of the size distributions, of approximately one order of magnitude for
411 much of the size range measured. This reflects the relative wide range of aerosol loadings
412 encountered during the campaign.

413 The measured number size distribution from each SLR has been fitted with multi-mode
414 lognormal functions:

415 $$\frac{dN}{d\log D_g} = \sum_i \frac{N_{tot,i}}{\sqrt{2\pi}\log\sigma_{g,i}} \left(-\frac{\left(\log D_p - \log D_{g,i}\right)^2}{2\log^2 \sigma_{g,i}} \right) \quad (4).$$

416 For each mode I, N_{tot} represents the total aerosol number concentration, D_g the median
417 diameter, and σ_g the geometric standard deviation. The logarithm refers to base 10. Size data
418 were fitted automatically using the MPCURVEFIT IDL routine available at
419 http://www.physics.wisc.edu/~craigm/idl/fitting.html. Since the aim of the fitting is to

Atmos. Chem. Phys. Discuss., doi:10.5194/acp-2016-47, 2016
Manuscript under review for journal Atmos. Chem. Phys.
Published: 11 April 2016

describe as closely as possible the measured number size distributions for subsequent optical calculations (Sect. 4.4), up to seven modes were used to fit the data. The parameters of the lognormal fits are reported in Table 3. The first mode of the size distribution is generally at 0.13-0.14 µm, whilst the largest mode is between ~5 and 8 µm for the different cases.

4.3 Spectral single scattering albedo: variability as a function of air mass origin and height

Figure 4 shows the spectral ω for the different SLRs considered in this study. Data have been separated based on the origin of the sampled air masses. The single scattering albedo varies in the range 0.84-0.98 at 370 nm and 0.70-0.99 at 950 nm and generally decreases with the wavelength, as it is typical for pollution particles (Dubovik et al., 2002). Only in two cases (V19_R1 and V30_R2) the single scattering albedo increases with wavelength. For these cases also very high values of ω are observed (0.92-0.97 for V19_R1 and 0.98-1.0 for V32_R2), which may suggest the possible mixing of pollution with sea spray. The lowest values of the single scattering albedo are measured for V27_R1 (0.84-0.70 between 370 and 950 nm) sampled at ~160 m and originated in the Open Sea sector. Data in Fig. 2 also indicate for V27_R1 very low values of $\Delta O_3/\Delta CO$ (~0.37) and a relatively high dN_{Aitken}/dN_{Acc} (~7), which suggests that V27_R1 is a fresh plume possibly associated to local emissions, i.e. ship plumes, over the basin. If we exclude V27_R1, the range of measured values appears comparable (within error bars) for the three considered sectors (Western, Eastern, and Open sea; ω between 0.88 and 0.98 at 370 nm and 0.83 and 0.99 at 950 nm.

The vertical variability of ω, together with dN_{Aitken}/dN_{Acc}, $\Delta O_3/\Delta CO$, SAE, and AAE, is shown in Fig. 5 for the different considered cases. With the only exception of V27_R1, for which the lowest values are observed below 200 m, the single scattering albedo does not show a clear trend with height, with a similar range of values measured in the boundary layer, below ~1000 m, and in the free troposphere up to ~3500 m. As for ω, the AAE does not significantly vary with height. At the same time, dN_{Aitken}/dN_{Acc} and SAE decrease with height, with a concurrent slight $\Delta O_3/\Delta CO$ increase, which may suggest an increase of plume age with height. The ensemble of these observations seems to indicate that, for our observed cases, the absorptivity properties of the sampled plumes do not depend on altitude and associated air mass age of the plume. It should be pointed out, however, that the majority of cases considered here have been sampled below 1000 m, so in the boundary layer, and the statistics in the free troposphere is only limited to a few events.

Atmos. Chem. Phys. Discuss., doi:10.5194/acp-2016-47, 2016
Manuscript under review for journal Atmos. Chem. Phys.
Published: 11 April 2016

Atmospheric Chemistry and Physics Discussions

Values of the single scattering albedo measured in this study are comparable with values reported at several other sites in the Central and Western Mediterranean region for pollution aerosols (Mallet et al., 2003 and 2013; Meloni et al., 2006; Saha et al., 2008; Di Biagio et al., 2009; Pandolfi et al., 2011). The single scattering albedo from these studies is observed to vary in the range 0.84-0.95 at 440 nm, 0.76-0.98 at 500-550 nm, and 0.80-0.87 at 870 nm. Compared with the literature, larger and lower values are obtained in the present study for few cases mostly influenced by sea spray and local fresh emissions, respectively.

4.4 Optical closure and estimation of the aerosol complex refractive index

As discussed in the previous section, the single scattering albedo of pollution aerosols shows a relatively large variability. Here we investigate the impact of this variability on the complex refractive index (m=n-ik) of the particles.

For eight selected SLRs for which both complete optical (scattering and absorption coefficients, and single scattering albedo) and size distribution measurements were available, the aerosol spectral complex refractive index has been estimated by optical closure study. These cases correspond to V19_R1, V21_R1, V21_R3, V23_R2, V27_R1, V31_R1, V32_R1, V32_R3 sampled within the boundary layer at <350 m altitude. The optical closure consisted in recalculating the spectral scattering σ_s and absorption σ_{abs} coefficients measured for each SLR by using the measured size distribution as input and by varying the real (n) and imaginary (k) parts of the complex refractive index in the calculations. Then, n and k are fixed when the best agreement between measurements and calculations is found. Optical calculations have been performed using Mie theory for spherical particles. The Mie_single.pro IDL routine available at http://www.atm.ox.ac.uk/code/mie/mie_single.html has been used. In the calculations the real part of the refractive index is varied in the range 1.30-1.80 at steps of 0.01, while the imaginary part in the range 0.001-0.1 at steps of 0.001, for a total of 5100 inversions for each SLR dataset. The uncertainty on the real and imaginary parts of the refractive index has been estimated with a sensitivity study. To this purpose, the values of n and k are also obtained by using as input the observed σ_s, σ_{abs}, and $\frac{dN}{d\log D_g}$ plus or minus one standard deviation on their measurement. The deviations of the values of n and k retrieved in the sensitivity study with respect to those obtained in the first inversions are assumed to correspond to the one standard deviation uncertainty. The estimated uncertainty is <5% for n and ~25-30% for k.

Atmos. Chem. Phys. Discuss., doi:10.5194/acp-2016-47, 2016
Manuscript under review for journal Atmos. Chem. Phys.
Published: 11 April 2016

The comparison of the measured and calculated σ_s and σ_{abs} are shown in Fig. 6, while the retrieved real and imaginary parts of the refractive index for the different SLRs are reported in Fig. 7. Data in Fig. 7 are also compared to the real and imaginary parts of the refractive index for the single components (insoluble, water soluble, soot, and sea salt) considered in the OPAC model (Optical Properties of Aerosols and Clouds, Hess et al., 1998) to represent continental, urban and maritime polluted aerosols.

As shown in Fig. 6, a very good agreement is found between the calculated and the measured scattering and absorption coefficients, with an average difference of less than 5% for both σ_s and σ_{abs}. For our analysed cases n and k vary in the range 1.67-1.75 and 0.003-0.038 at 370 nm and 1.41-1.75 and 0.002-0.068 at 950 nm, respectively. The imaginary part of the refractive index slightly increases with wavelength, while a decrease is observed for the real part in most cases. Highest values of k are obtained for V27_R1, which also shows the absolute lowest values of ω in our dataset (0.84-0.70), followed by V32_R1 and V32_R2, which also present relatively low values of ω (0.95-0.83). The lowest k, as well as among the lowest n, is instead obtained for V19_R1 (ω=0.92-0.96). The comparison of our data with OPAC values for single components suggests that in most cases particles are composed of a mixing of insoluble and water soluble components, with possible contributions of soot (V27_R1) ad sea salt (V19_R1). The results of the complex refractive index obtained in this study are in agreement with previous estimates obtained for pollution aerosols in continental Europe (n~1.50-1.72 and k~0.001-0.1 for UV-visible wavelengths e.g. Ebert et al., 2002, 2004; Müller et al., 2002; Mallet et al., 2003, 2011; Raut and Chazette, 2008). Larger values of both n and k are instead obtained here compared to AERONET retrievals at different sites in the Western Mediterranean (1.38-1.46 for n and 0.003-0.01 for k at 440 and 670 nm; Mallet et al., 2013).

Figure 8 shows the results of the correlation analysis between the single scattering albedo and the complex refractive index obtained for the analysed cases. For the real part, the range of retrieved n values is larger (1.41-1.70) for ω greater than ~0.95, while as the single scattering albedo decreases the real part converges to ~1.70-1.75 at all wavelengths. A strong correlation is observed between ω and k at all wavelengths, that is the lower the single scattering albedo, the higher the imaginary part. A linear regression fit was applied to the ω-k datasets at the seven wavelengths (R^2=0.83-0.95 at all wavelengths for the different fits). The intercept for all cases is lower than 1 (0.94-0.97), with lowest values (0.94) obtained at 880 and 950 nm. This is possibly associated to a slight underestimation of ω which, especially at

Atmos. Chem. Phys. Discuss., doi:10.5194/acp-2016-47, 2016
Manuscript under review for journal Atmos. Chem. Phys.
Published: 11 April 2016

these wavelengths, is difficult to determine given the high uncertainty on the particle absorption coefficient. Another source of uncertainty is the size distribution, which influences the results of Mie calculations, and thus has a direct impact on the refractive index retrieval.

4.5 Influence of the single scattering albedo variability on the aerosol direct shortwave radiative effect (DRE)

Radiative transfer model calculations with the GAME model have been performed with the aim of investigating the impact of the variable optical properties, and in particular the single scattering albedo, on the shortwave direct radiative effect of pollution particles in the Western Mediterranean basin.

Simulations have been performed by considering three different vertical aerosol profiles, based on observations reported by Di Biagio et al. (2015): i. aerosols only confined in the BL (whose altitude is fixed at 1000 m, in the mean of observations during TRAQA); ii. 50% of the aerosol optical depth in the BL and 50% in the FT (which is considered to extend between 1000 and 4000 m); iii. 20% of the aerosol optical depth in the BL and 80% in the FT. For the different cases we fixed the total aerosol optical depth at 0.2 at 550 nm, which corresponds to the mean of observations obtained over the Western basin during TRAQA (Di Biagio et al., 2015). However, results will be given as FE so they are independent on the chosen optical depth. We assume a uniform aerosol distribution and constant optical properties within the BL and the FT for the three different considered profiles. This assumption comes from the observations of the present study, which do not evidence any significant change of the aerosol properties with height. Aerosol spectral optical properties, both in the BL and in the FT up to 4000 m, are assumed from observations, as explained in the following.

The GAME model requires as input the aerosol optical depth, single scattering albedo, and asymmetry factor at 7 wavelengths between 330 and 1500 nm. The spectral optical depth between 330 and 1500 nm is extrapolated from the fixed value of 0.2 at 550 nm by assuming a Ångström exponent of 1.5, in the mean of our observations for pollution aerosols (see Fig. 2). For the single scattering albedo, we considered 3 different sets of values which correspond to the minimum, maximum, and mean of the values observed in this study (the absolute minimum for V27_R1 has been excluded for calculations since it represents an outlier in our data). The ω values at 370-950 nm as obtained from experimental data are then extrapolated at the 7 GAME wavelengths (Table 4). The asymmetry factor is calculated from Mie theory based on the refractive index values and size distribution data for the eight cases considered

Atmos. Chem. Phys. Discuss., doi:10.5194/acp-2016-47, 2016
Manuscript under review for journal Atmos. Chem. Phys.
Published: 11 April 2016

Atmospheric Chemistry and Physics Discussions

in the previous Section. The spectral variation of g used in the radiative transfer calculations is estimated as the mean of the values obtained for these eight cases extrapolated at the 7 GAME wavelengths. The obtained g varies between 0.60 at 330 nm and 0.51 at 1500 nm. These values are consistent with previous estimates of g obtained for pollution aerosols over the Mediterranean basin (Meloni et al., 2006; Saha et al., 2008; Mallet et al., 2011).

Background stratospheric aerosols (above 12 km) are also taken into account for radiative calculations; optical properties from the OPAC stratospheric aerosol model (Hess et al., 1998) are assumed.

Finally, in addition to aerosol optical properties, the GAME model requires as input the albedo of the surface (A_S) at 5 wavelengths between 448 nm and 2130 nm. In this study, simulations are performed over the sea surface. The albedo of the sea surface is obtained from Jin et al. (2004), which provide a parameterisation of A_S as a function of chlorophyll concentration (Chl), wind speed (w), aerosol optical depth at 500 nm (τ), and the solar zenith angle (θ). For this study A_S is estimated for Chl=0, w=6-9 m s^{-1}, τ=0.24 (extrapolated from the value of 0.2 at 550 nm), and θ=60°, and it varies between 0.009 and 0.005 in the considered 448-2130 nm spectral range.

Results of the radiative transfer simulations are shown in Fig. 9, which reports the FE at the surface, TOA, and atmosphere (FE_S, FE_{TOA} and FE_{ATM}) for the maximum, mean, and minimum of the single scattering albedo observed in this study. Results of the simulations are mostly independent on the vertical distribution of the aerosols (less than ~5% changes for FE_S, FE_{ATM}, and FE_{TOA} for the three different profiles used in the simulations), so the mean of the results obtained for the three cases is reported in Fig. 9. The forcing efficiency varies between -160 and -235 (FE_S), -137 and -92 (FE_{TOA}), and +23 and +143 (FE_{ATM}) W m^{-2} τ^{-1} for ω varying between its maximum and minimum values. Estimates of the forcing efficiencies in correspondence of the mean of ω are -198, -113, and +85 W m^{-2} τ^{-1} at the surface, TOA, and atmosphere, respectively. The corresponding instantaneous shortwave heating rate at the surface varies between 0.2 and 2.0 K day^{-1} for ω between its maximum and minimum.

As expected, the lower the single scattering albedo, the larger in absolute value the FE_S and FE_{ATM} and the lower the FE_{TOA}. This is due to the impact of absorption on the amount of radiation trapped in the atmosphere and transmitted towards the surface, which thus enhance the radiative effect in the atmosphere and at the surface for decreasing ω. Conversely, the larger the particle absorption, the lower the effect on the radiation reflected back to space, and thus the decrease of the intensity of the cooling effect at the TOA. Changes in the single

Atmos. Chem. Phys. Discuss., doi:10.5194/acp-2016-47, 2016
Manuscript under review for journal Atmos. Chem. Phys.
Published: 11 April 2016

Atmospheric Chemistry and Physics Discussions

scattering albedo of the particles between its maximum and minimum ($\Delta\omega$=0.1-0.2 at the different wavelengths) determine about a 50% strengthening of the direct shortwave radiative effect at the surface, and a reduction of ~30% the effect at the TOA. Consequently, the atmospheric FE may vary up to an order of magnitude. These results thus highlight the sensitivity of the DRE on the absorptivity properties of the particles, as well as the importance of accurately reproducing the single scattering albedo of aerosols to correctly evaluate their direct radiative effect.

The results of the present study are in quite good agreement with previous estimates of the aerosol forcing efficiency for pollution aerosols in the Mediterranean area. FE_S, FE_{ATM}, and FE_{TOA} obtained here compare well with data obtained in the Central Mediterranean by Di Biagio et al. (2009, 2010), who provide estimates based only on observational data, i.e. without any assumption on the aerosol optical properties. In these studies they report a forcing efficiency of ~-200 and -164 W m^{-2} τ^{-1} at the surface and TOA at solar zenith angles of 50°-60° for mixed aerosols (pollution plus sea salt particles). They estimate an increase in absolute value of FE_S of about 20-40% due to a decrease of 0.1-0.2 of the single scattering albedo (at 415 and 868 nm) of the aerosols, as well as a concurrent increase of FE_{TOA} of about 10-40%. The observations obtained in this study fall in the range of variability reported by Di Biagio et al. (2009, 2010). Our data also agree with estimates of Saha et al. (2008), reporting for pollution aerosols measured in the French Mediterranean coast up to 40% variability in the FE_S and FE_{TOA}, concurrently with 70% increase of FE_{ATM}, due to a ω change of 0.15 at 525 nm. Conversely, our estimates at the surface and TOA are larger in absolute value compared to data reported for continental Europe by Horvath et al. (2002), who estimated a FE_S of ~-164 W m^{-2} τ^{-1} and a FE_{TOA} of -50 W m^{-2} τ^{-1} for polluted aerosols with ω=0.90 at 520 nm, thus comparable with our mean values of single scattering albedo for pollution aerosols.

5. Conclusions

In this study we have presented measurements of the spectral optical properties (scattering and absorption coefficients and single scattering albedo) and particle size distributions for pollution aerosols obtained over the remote sea in the Western Mediterranean basin during the TRAQA campaign in summer 2012. The set of observations analysed in this study can be assumed to be representatives of a wide range of different conditions that can be observed over the basin, both in terms of pollution sources, aerosol loadings, and lifetimes of the

Atmos. Chem. Phys. Discuss., doi:10.5194/acp-2016-47, 2016
Manuscript under review for journal Atmos. Chem. Phys.
Published: 11 April 2016

Atmospheric Chemistry and Physics Discussions

plumes. The detailed characterization of the spectral optical properties of pollution aerosols in the Western basin was missing to date.

Observations from the present study show a large variability of the optical properties of pollution aerosols over the basin, in particular of the spectral single scattering albedo. Values of ω in the range 0.84-0.98 at 370 nm and 0.70-0.99 at 950 nm are observed in this study. This variability of ω does not seem to be clearly linked neither to the particle origin, nor to the altitude and associated ageing of the sampled plumes. The variability of ω reflects in a large variability for the complex refractive index of pollution aerosols, which is estimated to span in the range 1.41-1.75 for the real part and 0.002-0.068 for the imaginary part between 370 and 950 nm. The analysis of the complex refractive index suggests that possible differences in terms of particle compositions can explain in part the observed variability of ω. A large range of compositions has been however reported for pollution aerosols in Europe and the Mediterranean basin (Mallet et al., 2003; Ebert et al., 2004; Pey et al., 2010; Piazzola et al., 2012) and a more detailed analysis of the composition for the cases obtained in this study should be addressed.

Based on the observations of the present study, the variability of optical properties for pollution aerosols can arise from the combination of different factors, linked to the origin, production mechanism, and ageing of the plumes along their lifetime, as well as the possible mixing of different plumes with different characteristics. So, the inherent heterogeneity of sources, coexistence of different air masses, and multiple physical and chemical processes occurring in a complex environment such as the Western Mediterranean may give rise to this inherent variability of the particle single scattering albedo.

This observed variability on ω has a large influence on the direct shortwave radiative effect of pollution aerosols at the surface, TOA, and within the atmosphere. For instance, a change of up to an order of magnitude (from +23 to +143 W m^{-2} τ^{-1} at 60° solar zenith angle) in the atmospheric radiative effect is estimated due to the variability of the single scattering albedo within the range of values observed in this study. The change in the amount of atmospheric absorbed solar radiation may have a strong impact on the temperature profile and the atmospheric thermal structure, with important consequences on several processes, such as cloud formation and precipitations. The strong sensitivity of the DRE also at the surface, up to 50% for varying ω, on its turn, may largely impact the rate of evaporation over the basin, which is also a crucial component of the hydrological cycle (Nabat et al., 2015). Given the large sensitivity of the Mediterranean area and the high risk of desertification for this region

(Giorgi and Lionello, 2008; IPCC, 2013) any factor possibly impacting the hydrological cycle should be taken carefully into account by regional climate models. In this view, results from the present study can be used to provide a constraint of the absorption properties of pollution particles in the Western Mediterranean basin to use in regional modelling studies. Constraining these properties constitutes a crucial step in order to better assess the role of aerosols on the radiative balance of this region and to ameliorate the capability of making projection on future climate changes.

Author contributions

J.-L. Attié, F. Ravetta, G. Ancellet, and P. Formenti designed the TRAQA experiment and coordinated the campaign. C. Gaimoz, N. Grand, and C. Di Biagio operated the instruments on board the ATR-42 during the flights. C. Di Biagio performed the data analysis with contributions from L. Doppler and P. Formenti. S. Bucci and F. Fierli performed the FLEXPART simulations. M. Mallet and P. Dubuisson provided the GAME code for radiative calculations. C. Di Biagio wrote the manuscript with contributions from the co-authors.

Acknowledgements

All measurement presented here are from the Chemistry-Aerosol Mediterranean Experiment project (ChArMEx, http://charmex.lsce.ipsl.fr), which is the atmospheric component of the French multidisplinary program MISTRALS (Mediterranean Integrated Studies aT Regional And Local Scales). ChArMEx-France was principally funded by INSU, ADEME, ANR, CNES, CTC (Corsica region), EU/FEDER, Météo-France, and CEA. TRAQA was funded by ADEME/PRIMEQUAL and MISTRALS/ChArMEx programmes and Observatoire Midi-Pyrénées. C. Di Biagio thanks the Centre National des Etudes Spatiales (CNES) for financial support.

The authors wish to thank the technicians, pilots and ground crew of SAFIRE (Service des Avions Francais Instruments pour la Recherche en Environnement) for facilitating the instrument integration and conducting flying operations. We thank S. Chevaillier, R. Loisil, J. Pelon, and P. Zapf for their contribution during the campaign. We also wish to thank G. Siour for his help to run the GAME radiative code.

Atmos. Chem. Phys. Discuss., doi:10.5194/acp-2016-47, 2016
Manuscript under review for journal Atmos. Chem. Phys.
Published: 11 April 2016

Atmospheric Chemistry and Physics Discussions

References

Anderson, T. L. and Ogren, J. A.: Determining aerosol radiative properties using the TSI 3563 integrating nephelometer, Aerosol Sci. Technol., 29, 57–69, 1998.

Arnott, W., Hamasha, K., Moosm¨uller, H., Sheridan, P. J. , and Ogren, J. A.: Towards aerosol light-absorption measurements with a 7-wavelength aethalometer: Evaluation with a photoacoustic instrument and 3-wavelength nephelometer, Aerosol Sci. Tech., 39(1), 17–29, 2005.

Boucher, O., et al., Clouds and Aerosols. Stocker, T., & Qin, D. (eds), Climate Change 2013: The Physical Science Basis. Contribution of Working Group I to the Fifth Assessment Report of the Intergovernmental Panel on Climate Change. Cambridge Univ. Press, Cambridge, United Kingdom and New York, NY, USA, 2013.

Brioude, J., Arnold, D., Stohl, A., Cassiani, M., Morton, D., Seibert, P., Angevine, W., Evan, S., Dingwell, A., Fast, J. D., Easter, R. C., Pisso, I., Burkhart, J., and Wotawa, G.: The Lagrangian particle dispersion model FLEXPART-WRF version 3.1, Geosci. Model Dev., 6, 1889-1904, doi:10.5194/gmd-6-1889-2013, 2013.

Collaud Coen, M., Weingartner, E., Apituley, A., Ceburnis, D., Fierz-Schmidhauser, R., Flentje, H., Henzing, J. S., Jennings, S. G., Moerman, M., Petzold, A., Schmid, O., and Baltensperger, U.: Minimizing light absorption measurement artifacts of the Aethalometer: evaluation of five correction algorithms, Atmos. Meas. Tech., 3, 457–474, doi:10.5194/amt-3-457-2010, 2010.

Di Biagio, C., di Sarra, A., Meloni, D., Monteleone, F., Piacentino, S., and Sferlazzo, D.: Measurements of Mediterranean aerosol radiative forcing and influence of the single scattering albedo, J. Geophys. Res., 114, D06211, doi:10.1029/2008JD011037, 2009.

Di Biagio, C., di Sarra, A., and D. Meloni, D.: Large atmospheric shortwave radiative forcing by Mediterranean aerosol derived from simultaneous ground-based and spaceborne observations, and dependence on the aerosol type and single scattering albedo, J. Geophys. Res., 115, D10209, doi: 10.1029/2009JD012697, 2010.

Di Biagio, C., Doppler, L., Gaimoz, C., Grand, N., Ancellet, G., Raut, J.-C., Beekmann, M., Borbon, A., Sartelet, K., Attié, J.-L., Ravetta, F., and Formenti, P.: Continental pollution in the western Mediterranean basin: vertical profiles of aerosol and trace gases measured over the sea during TRAQA 2012 and SAFMED 2013, Atmos. Chem. Phys., 15, 9611-9630, doi:10.5194/acp-15-9611-2015, 2015.

Dubovik, O., Holben, B., Eck, T. F., Smirnov, A., Kaufman, Y. J., King, M. D., Tanré, D., and Slutsker, I.: Variability of absorption and optical properties of key aerosol types observed in worldwide locations, J. Atmos. Sci., 59, 590–608, 2002.

Dubuisson, P., Buriez, J. C. and Fouquart, Y.: High spectral resolution solar radiative transfer in absorbing and scattering media: Application to the satellite simulation, J. Quant. Spectrosc. Radiat. Transfer, 55, 103–126, 1996.

Dubuisson, P., Roger, J., Mallet, M., and Dubovik, O.: A Code to Compute the Direct Solar Radiative Forcing: Application to An- thropogenic Aerosols during the Escompte Experiment, Proc. In- ternational Radiation Symposium (IRS 2004) on Current Prob- lems in Atmospheric Radiation, edited by: Fischer, H., Sohn, B.- J., and Deepak, A., Hampton, 127–130, 23–28 August 2004, Bu- san, Korea, 2006.

Ebert, M., Weinbruch, S., Rausch, A., Gorzawski, G., Hoffmann, P., Wex, H., and Helas, G.: The complex refractive index of aerosols during LACE 98 as derived from the analysis of individual particles, J. Geophys. Res., 107, D21, 8121, doi:10.1029/2000JD000195, 2002.

Ebert, M., Weinbruch, S., Hoffmann, P., and Ortner, H. M.: The chemical composition and complex refractive index of rural and urban influenced aerosols determined by individual particle analysis, Atmos. Environ., 38, 6531–6545, 2004.

729 Estellés, V., Martínez-Lozano, J. A., Utrillas, M. P., and Campanelli, M.: Columnar aerosol properties
730 in Valencia (Spain) by ground-based Sun photometry, J. Geophys. Res., 112, D11201,
731 doi:10.1029/2006JD008167, 2007.

732 Esteve, A. R., Ogren, J. A., Sheridan, P. J., Andrews, E., Holben, B. N., and Utrillas, M. P.: Sources
733 of discrepancy between aerosol optical depth obtained from AERONET and in-situ aircraft
734 profiles, Atmos. Chem. Phys., 12, 2987-3003, doi:10.5194/acp-12-2987-2012, 2012.

735 Giorgi, F., and Lionello, P.: Climate change projections for the Mediterranean region. Global Planet
736 Change, 63, 90-104. doi:10.1016/j.gloplacha.2007.09.005, 2008.

737 Gkikas, A., Houssos, E. E., Hatzianastassiou, N., Papadimas C. D., and Bartzokas, A.: Synoptic
738 conditions favouring the occurrence of aerosol episodes over the broader Mediterranean basin Q. J.
739 R. Meteorol. Soc. 138: 932–949, 2012.

740 Hess, M., Koepke, P., and Schult, I.: Optical properties of aerosols and clouds: The software package
741 OPAC, Bull. Am. Meteorol. Soc, 79, 831–844, 1998.

742 Horvath, H., Alados Arboledas, L., Olmo, F. J., Jovanovic, O., Gangl, M., Sanchez, C., Sauerzopf, H.,
743 and Seidl, S.: Optical characteristics of the aerosol in Spain and Austria and its effect on radiative
744 forcing, J. Geophys. Res., 107, 4386, doi: 10.1029/2001JD001472, 2002.

745 IPCC, 2013: Climate Change 2013: The Physical Science Basis. Contribution of Working Group I to
746 the Fifth Assessment Report of the Intergovernmental Panel on Climate Change [Stocker, T.F., D.
747 Qin, G.-K. Plattner, M. Tignor, S.K. Allen, J. Boschung, A. Nauels, Y. Xia, V. Bex and P.M.
748 Midgley (eds.)]. Cambridge University Press, Cambridge, United Kingdom and New York, NY,
749 USA, 1535 pp, doi:10.1017/CBO9781107415324.

750 Jin, Z., Charlock, T. P., Smith Jr., W. L., and Rutledge, K.: A parametrization of ocean surface
751 albedo, Geophys. Res. Lett., 31, L22301, doi:10.1029/2004GL021180, 2004.

752 Lelieveld, J., Berresheim, H., Borrmann, S., et al.: Global air pollution crossroads over the
753 Mediterranean, Science, 298, 794–799, 2002.

754 Liu, Y. and Daum, P.: The effect of refractive index on size distributions and light scattering
755 coefficients derived from optical particle counters, J. Aerosol Sci., 31, 945–957, 2000.Loeb, N. G.,
756 and Su, W.: Direct Aerosol Radiative Forcing Uncertainty Based on a Radiative Perturbation
757 Analysis, J. Climate, 23, 5288–5293. doi: http://dx.doi.org/10.1175/2010JCLI3543.1, 2010.

758 Loeb, N. G., and Su, W. Y.: Direct aerosol radiative forcing uncertainty based on a radiative
759 perturbation analysis, J. Clim., 23, 5288–5293, 2010.

760 Lyamani, , H., Olmo, F. J., Alcántara, A., and Alados-Arboledas, L.: Atmospheric aerosols during the
761 2003 heat wave in southeastern Spain. I: Spectral optical depth, Atmos. Environ., *40*, 6453–6464,
762 2006.

763 Lyamani, H., Valenzuela, A., Perez-Ramirez, D., Toledano, C., Granados-Muñoz, M. J., Olmo, F. J.,
764 and Alados-Arboledas, L.: Aerosol properties over the western Mediterranean basin: temporal and
765 spatial variability, Atmos. Chem. Phys., 15, 2473-2486, doi:10.5194/acp-15-2473-2015, 2015

766 Mallet, M., Roger, J. C., Despiau, S., Dubovik, O., and Putaud, J. P.: Microphysical and optical
767 properties of aerosol particles in urban zone during ESCOMPTE, Atmos. Res., 69, 73–97, 15
768 2003.

769 Mallet, M., Van Dingenen, R., Roger, J. C., Despiau, S., and Cachier, H.: In situ airborne
770 measurements of aerosol optical properties during photochemical pollution events, J. Geophys.
771 Res., 110, D03205, doi:10.1029/2004JD005139, 2005.

772 Mallet, M., Gomes, L., Solmon, F., Sellegri, K., Pont, V., Roger, J. C., Missamou, T., and Piazzola, J.:
773 Calculation of key optical properties of the main anthropogenic aerosols over the Western French
774 coastal Mediterranean Sea, Atmos. Res., 101, 396–411, 2011.

775 Mallet, M., Dubovik, O., Nabat, P., Dulac, F., Kahn, R., Sciare, J., Paronis, D., and Léon, J. F.:
776 Absorption properties of Mediterranean aerosols obtained from multi-year ground-based remote
777 sensing observations, Atmos. Chem. Phys., 13, 9195-9210, doi:10.5194/acp-13-9195-2013, 2013.

778 McComiskey, A., Schwartz, S. E., Schmid, B., Guan, H., Lewis, E. R., Ricchiazzi, P., and Ogren,
779 J. A.: Direct aerosol forcing: Calculation from observables and sensitivities to inputs, J.
780 Geophys. Res., 113, D09202, doi:10.1029/2007JD009170, 2008.

781 Meloni, D., di Sarra, A., Pace, G., and Monteleone, F.: Aerosol optical properties at Lampedusa
782 (Central Mediterranean). 2. Determination of single scattering albedo at two wavelengths for
783 different aerosol types, Atmos. Chem. Phys., 6, 715-727, doi:10.5194/acp-6-715-2006, 2006.

784 Millán, M. M., Mantilla, E., Salvador, R., Carratala, A., Sanz, M. J., Alonso, L., Gangoiti, G., and
785 Navazo, M.: Ozone cycles in the western Mediterranean basin: interpretation of monitoring data in
786 complex terrain, J. Appl. Meteorol., 4, 487–507, 2000.

787 Müller, D., Ansmann, A., Wagner, F., Franke, K., and Althausen, D.: European pollution outbreaks
788 during ACE 2: Microphysical particle properties and single-scattering albedo inferred from
789 multiwavelength lidar observations, J. Geophys. Res., 107, D15, 4248, 10.1029/2001JD001110,
790 2002.

791 Nabat, P., Somot, S., Mallet, M., Sevault, F., Chiacchio, M. and Wild, M.: Direct and semi-direct
792 aerosol radiative effect on the Mediterranean climate variability using a coupled Regional Climate
793 System Model Clim. Dyn., 44, 1127-1155, doi:10.1007/s00382-014-2205-6, 2015.

794 Nedélec, P., Cammas, J.-P., Thouret, V., Athier, G., Cousin, J.-M., Legrand, C., Abonnel, C.,
795 Lecoeur, F., Cayez, G., and Marizy, C.: An improved infrared carbon monoxide analyser for
796 routine measurements aboard commercial Airbus aircraft: technical validation and first scientific
797 results of the MOZAIC III programme, Atmos. Chem. Phys., 3, 1551–1564, doi:10.5194/acp-3-
798 1551-2003, 2003.

799 Pace, G., di Sarra, A., Meloni, D., Piacentino, S., Chamard, P.: Aerosol optical properties at
800 Lampedusa (Central Mediterranean). 1. Influence of transport and identification of different
801 aerosol types, Atmos. Chem. Phys., 6, 697–713, 2006.

802 Pandolfi, M., Cusack, M., Alastuey, A., and Querol, X.: Variability of aerosol optical properties in the
803 Western Mediterranean Basin Atmos. Chem. Phys., 11, 8189–8203, 2011.

804 Pandolfi, M., et al.: Effects of sources and meteorology on particulate matter in the Western
805 Mediterranean Basin: An overview of the DAURE campaign, J. Geophys. Res. Atmos., 119,
806 4978–5010, doi:10.1002/2013JD021079, 2014.

807 Pérez, N., Pey, J., Castillo, S., Viana, M., Alastuey, A., and Querol, X.: Interpretation of the
808 variability of levels of regional background aerosols in the Western Mediterranean, Sci. Tot.
809 Environ., 407, 527–540, 2008.

810 Pey, J., Querol, X., and Alastuey, A.: Discriminating the regional and urban contributions in the
811 North-Western Mediterranean: PM levels and composition, Atmos Environ, 44, 1587–96, 2010.

812 Piazzola, J., Sellegri, K., Bourcier, L., Mallet, M., Tedeschi, G., and Missamou, T.: Physicochemical
813 characteristics of aerosols measured in the spring time in the Mediterranean coastal zone, Atmos.
814 Environ., 54, 545-556, 2012.

815 Ramana, M. V., and Ramanathan, V.: Abrupt transition from natural to anthropogenic aerosol
816 radiative forcing: Observation at the ABCMaldives Climate Observatory, J. Geophys. Res., 111,
817 D20207, doi:10.1029/2006JD007063, 2006.

818 Raut, J.-C., and Chazette, P.: Vertical profiles of urban aerosol complex refractive index in the frame
819 of ESQUIF airborne measurements, Atmos. Chem. Phys., 8, 901–919, 2008.Russell, P. B.,
820 Bergstrom, R. W., Shinozuka, Y., Clarke, A. D., DeCarlo, P. F., Jimenez, J. L., Livingston, J. M.,
821 Redemann, J., Dubovik, O., and Strawa, A.: Absorption Angstrom Exponent in AERONET and

related data as an indicator of aerosol composition, Atmos. Chem. Phys., 10, 1155–1169, doi:10.5194/acp-10-1155-2010, 2010.

Saha, A., Mallet, M., Roger, J. C., Dubuisson, P., Piazzola, J., and Despiau, S.: One year measurements of aerosol optical properties over an urban coastal site: Effect on local direct radiative forcing, Atmos. Res., *90*, 195-202, 2008.

Stamnes K., Tsay, S. C., Wiscombe, W., and Jayaweera, K.: Numerically stable algorithm for discrete-ordinate-method radiative transfer in multiple scattering and emitting layered media, Appl. Opt., 27, 2502–2509, 1988.

Stier, P., Schutgens, N. A. J., Bellouin, N., Bian, H., Boucher, O., Chin, M., Ghan, S., Huneeus, N., Kinne, S., Lin, G., Ma, X., Myhre, G., Penner, J. E., Randles, C. A., Samset, B., Schulz, M., Takemura, T., Yu, F., Yu, H., and Zhou, C.: Host model uncertainties in aerosol radiative forcing estimates: results from the AeroCom Prescribed intercomparison study, Atmos. Chem. Phys., 13, 3245-3270, doi:10.5194/acp-13-3245-2013, 2013.

Stohl, A., Hittenberger, M., and Wotawa, G.: Validation of the Lagrangian particle dispersion model Flexpart against large-scale tracer experiment data, Atmos. Environ., 32, 4245–4264, 1998.

Weingartner, E., Saathof, H., Schnaiter, M., Streit, N., Bitnar, B., and Baltensperger, U.: Absorption of light by soot particles: Determination of the absorption coefficient by means of Aethalometers, J. Aerosol Sci., 34, 1445–1463, 2003.

Atmos. Chem. Phys. Discuss., doi:10.5194/acp-2016-47, 2016
Manuscript under review for journal Atmos. Chem. Phys.
Published: 11 April 2016

Atmospheric Chemistry and Physics Discussions

863 # Tables
864

865 **Table 1.** Summary of information on the SLRs analysed in this study. The SLR location
866 (within the boundary layer or in the free troposphere) has been determined based on the
867 boundary layer top height estimated for the closest vertical sounding performed during each
868 flight (see Di Biagio et al., 2015). The Sector of origin for sampled air masses has been
869 determined based on FLEXPART back-trajectories.
870

Flight number	SLR_ID	Date	Time start-stop	Altitude (m)	Location	Sector of origin
V19	V19_R1	26/06/2012	11:23-11:38	322	Within the boundary layer	Eastern
V19	V19_R2	26/06/2012	11:44-11:59	897	Within the boundary layer	Eastern
V21	V21_R1	27/06/2012	10:54-11:12	312	Within the boundary layer	Eastern
V21	V21_R2	27/06/2012	11:48-12:04	629	Within the boundary layer	Eastern
V21	V21_R3	27/06/2012	12:05-12:19	311	Within the boundary layer	Western
V22	V22_R1	29/06/2012	7:42-8:01	478	Within the boundary layer	Eastern
V23	V23_R2	29/06/2012	12:05-12:20	319	Within the boundary layer	Open Sea
V25	V25_R1	04/07/2012	9:08-9:24	639	Within the boundary layer	Western
V25	V25_R2	04/07/2012	9:32-9:48	2015	Free troposphere	Western
V25	V25_R3	04/07/2012	9:50-10:08	2538	Free troposphere	Western
V26	V26_R2	04/07/2012	17:08-17:25	1877	Free troposphere	Western
V27	V27_R1	06/07/2012	9:28-9:47	164	Within the boundary layer	Open Sea
V28	V28_R2	06/07/2012	15:58-16:13	927	Within the boundary layer	Open Sea
V30	V30_R1	07/07/2012	14:09-14:28	3498	Free troposphere	Western
V30	V30_R2	07/07/2012	14:51-15:07	549	Within the boundary layer	Open Sea
V31	V31_R1	10/07/2012	15:44-16:20	322	Within the boundary layer	Western
V31	V31_R2	10/07/2012	16:31-16:59	954	Within the boundary layer	Western
V32	V32_R1	11/07/2012	12:52-13:13	250	Within the boundary layer	Western
V32	V32_R2	11/07/2012	13:22-13:48	788	Within the boundary layer	Western
V32	V32_R3	11/07/2012	14:02-14:12	336	Within the boundary layer	Western
V32	V32_R4	11/07/2012	14:18-14:35	802	Within the boundary layer	Western

871

872

Atmos. Chem. Phys. Discuss., doi:10.5194/acp-2016-47, 2016
Manuscript under review for journal Atmos. Chem. Phys.
Published: 11 April 2016

Atmospheric Chemistry and Physics Discussions

Table 2. Summary of the aerosol in situ measurements on the ATR-42 during the TRAQA campaign. Details on the data treatment and uncertainty estimation for the different instruments are provided in Sect. 2.

Property measured	Instrument	Location on aircraft	Flow rate (l min^{-1})	Time resolution	Size range	Sensitivity or uncertainty	Comments
Aerosol number concentration	Condensation Particle Counter (CPC 3775)	in the cabin behind AVIRAD inlet	1.5	5 sec	0.004 – 3 µm	±10% (concentration)	
Aerosol size distribution	Passive cavity aerosol spectrometer probe (PCASP 100x)	aircraft fuselage, left side before the wing	0.06	1 sec	Nominally 0.1 – 3.0 µm Corrected for refractive index 0.10 – 4.47 µm	<±25% (diameter optical to geometric conversion) ±15% (concentration) (e.g., Highwood et al., 2012)	Aerosol concentration underestimated by 50% between 0.4 and 1.0 µm
	SkyGRIMM 1.129	in the cabin behind AVIRAD inlet	1.3	6 sec	Nominally 0.3 – 32 µm Corrected for refractive index 0.28 – 65.80 µm (AVIRAD 50% cut-off efficiency at ~12 µm diameter)	<±25% (diameter optical to geometric conversion) ±10% (concentration)	Data not available >350 m
Dry aerosol scattering coefficient σ_s (450, 550, 700 nm)	TSI 3563 integrating nephelometer	in the cabin behind AVIRAD inlet	30	6 sec	50% cut-off efficiency at ~ 12 µm diameter	<±10% for σ_s at 450, 550, and 700 nm	
Aerosol absorption coefficient (σ_a) (370, 470, 520, 590, 660, 880, 950 nm)	Magee AE31 aethalometer	in the cabin behind AVIRAD inlet	13	2 min	50% cut-off efficiency at ~12 µm diameter	11-70% variable at the different wavelengths	Data available only for 60% of SLRs

Atmos. Chem. Phys. Discuss., doi:10.5194/acp-2016-47, 2016
Manuscript under review for journal Atmos. Chem. Phys.
Published: 11 April 2016

Atmospheric Chemistry and Physics Discussions

881 **Table 3.** Lognormal mode parameters of the measured aerosol size distribution (total aerosol
882 number concentration, N_{tot}, median diameter, D_g, and geometric standard deviation, σ_g). Data
883 corresponds to SLRs below ~350 m altitude. Diameters are given in microns and number
884 concentrations refer to ambient conditions.
885

		Mode 1	Mode 2	Mode 3	Mode 4	Mode 5	Mode 6	Mode 7
V19_R1	N_{tot}	498.00	160.00	20.00	4.50	1.95	0.10	
	D_g	0.13	0.24	0.38	0.66	1.55	4.85	
	σ_g	1.19	1.16	1.17	1.29	1.60	1.38	
V21_R1	N_{tot}	600.00	210.00	29.00	5.50	0.55		
	D_g	0.13	0.24	0.37	0.52	1.56		
	σ_g	1.20	1.17	1.15	1.40	1.62		
V21_R3	N_{tot}	600.00	195.00	30.00	2.80	0.48	0.02	
	D_g	0.13	0.23	0.37	0.57	1.55	4.95	
	σ_g	1.19	1.16	1.18	1.33	1.66	1.41	
V23_R2	N_{tot}	660.00	195.00	25.00	3.20	0.75	0.03	
	D_g	0.13	0.23	0.37	0.57	1.59	5.69	
	σ_g	1.19	1.16	1.16	1.37	1.69	1.33	
V27_R1	N_{tot}	930.00	264.00	40.00	4.60	0.52	0.04	0.004
	D_g	0.13	0.23	0.37	0.55	1.57	3.85	8.20
	σ_g	1.19	1.17	1.18	1.38	1.68	1.12	1.26
V31_R1	N_{tot}	482.00	278.00	48.00	2.70	0.55	0.01	
	D_g	0.14	0.24	0.35	0.54	1.82	7.14	
	σ_g	1.20	1.16	1.17	1.39	1.65	1.17	
V32_R1	N_{tot}	1135.00	413.00	55.00	5.00	0.65	0.01	
	D_g	0.13	0.23	0.37	0.50	1.65	7.30	
	σ_g	1.19	1.18	1.16	1.37	1.66	1.11	
V32_R3	N_{tot}	235.00	84.00	12.00	1.80	0.12	0.02	0.004
	D_g	0.14	0.23	0.38	0.50	1.57	3.75	7.99
	σ_g	1.19	1.16	1.16	1.32	1.68	1.12	1.31

886
887
888

889 **Table 4.** Maximum, mean, and minimum of the single scattering albedo considered for radiative
890 transfer calculations. Values are reported at the 7 wavelengths used as inputs in the GAME model.

	330 nm	400 nm	550 nm	670 nm	870 nm	1020 nm	1500 nm
SSA max	0.98	0.98	0.99	0.99	1.00	0.99	0.99
SSA mean	0.93	0.93	0.92	0.91	0.90	0.90	0.89
SSA min	0.88	0.87	0.85	0.85	0.83	0.82	0.80

891
892
893
894

Atmos. Chem. Phys. Discuss., doi:10.5194/acp-2016-47, 2016
Manuscript under review for journal Atmos. Chem. Phys.
Published: 11 April 2016

Atmospheric Chemistry and Physics Discussions

Figures

Figure 1. Upper panel: geographical position of the different straight levelled runs (SLRs) performed during the TRAQA campaign and analysed in this paper. The label for each point in the figure identifies the flight number and the corresponding SLR: for example V22_R1 indicates the coordinates of the first SLR of flight V22. Lower panel: definition of three different source areas for the various SLRs (see Sect. 3.1 for more details). The Western sector includes trajectories coming from the Atlantic Ocean and travelling over France or northern Spain before reaching the Western basin; the Eastern sector includes air mass trajectories from continental Europe that have travelled over northern Italy-Po Valley before entering the basin; and the Open Sea sector consists of trajectories which have experienced at least 2 days of subsidence over the sea in the Western basin.

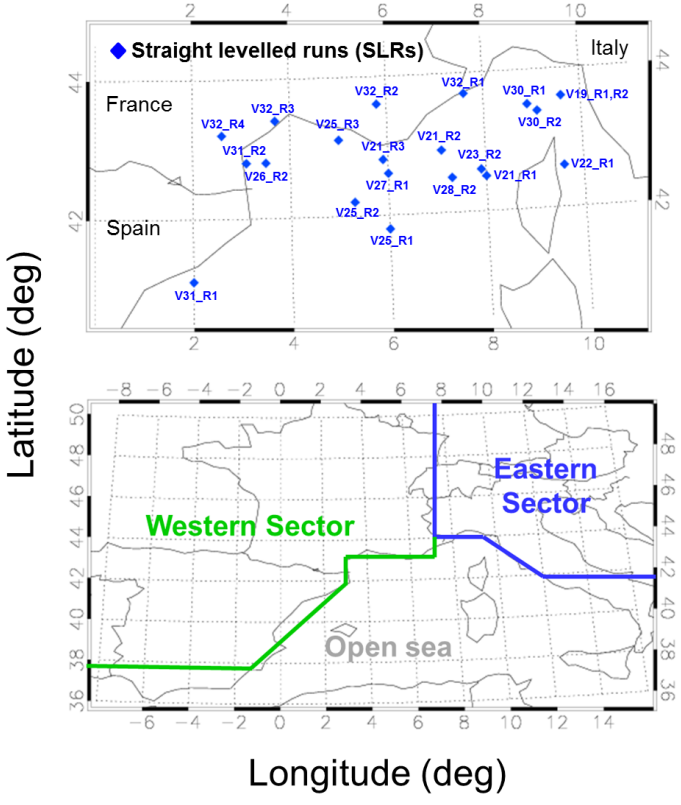

Atmos. Chem. Phys. Discuss., doi:10.5194/acp-2016-47, 2016
Manuscript under review for journal Atmos. Chem. Phys.
Published: 11 April 2016

Atmospheric Chemistry and Physics Discussions

910 **Figure 2.** Averages over the different TRAQA straight levelled runs (SLRs) of the measured:
911 altitude, spectral scattering coefficient (σ_s; 450, 550, and 700 nm), scattering Ångström exponent
912 (SAE), spectral absorption coefficient (σ_{abs}; 370, 470, 520, 590, 660, 880, and 950 nm), absorption
913 Ångström exponent (AAE), ozone enhancement factor ($\Delta O_3/\Delta CO$) and Aitken-to-accumulation
914 ratio (dN_{Aitken}/dN_{Acc}). Uncertainties indicate the 1-σ standard deviation. The x-axis indicates the
915 flight number (19 to 32 for flights V019 to V032); each point for the same flight number represents
916 a different SLR.
917
918

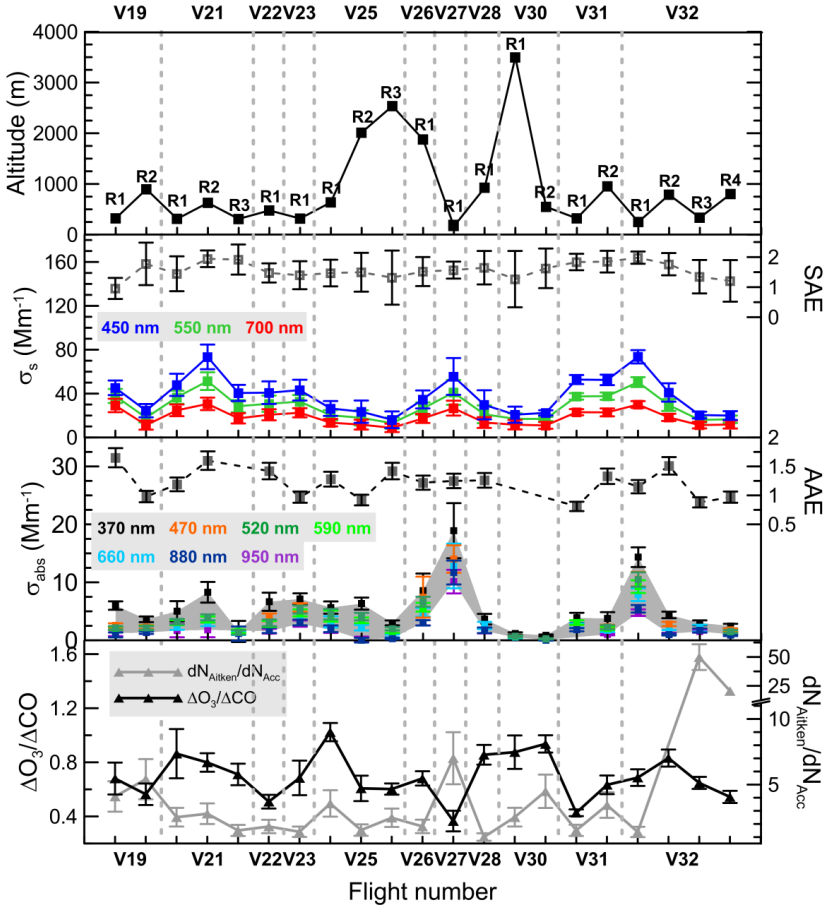

919
920
921
922
923

Atmos. Chem. Phys. Discuss., doi:10.5194/acp-2016-47, 2016
Manuscript under review for journal Atmos. Chem. Phys.
Published: 11 April 2016

Atmospheric Chemistry and Physics Discussions

924 **Figure 3.** Number size distributions (left panel) and volume size distributions (right panel)
925 measured over the different SLRs for the TRAQA flights. Data corresponds to measurements
926 performed within the boundary layer at altitudes <350 m (V19_R1, V21_R1, V21_R3, V23_R2,
927 V27_R1, V31_R1, V32_R1, V32_R3). Concentrations are given at ambient conditions. Grey
928 shading represents minimum and maximum measured values, while the black curve is the average
929 size. Measurement uncertainties are also reported for the average curve.
930
931

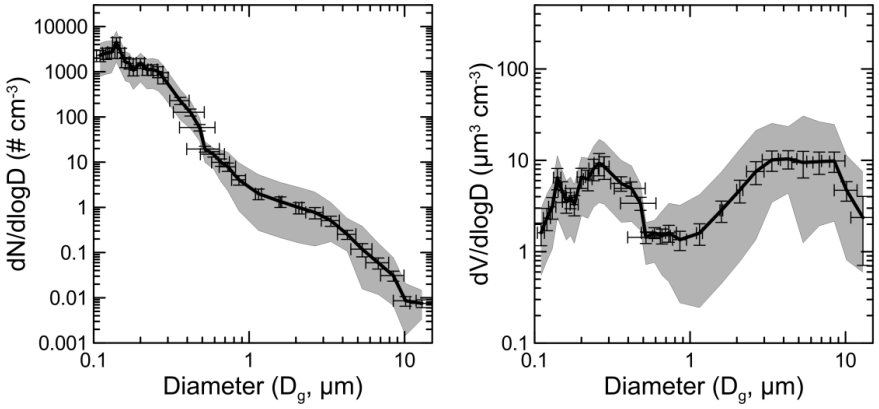

932
933

934 **Figure 4.** Spectral single scattering albedo at seven wavelengths between 370 and 950 nm
935 calculated from nephelometer and aethalometer measurements for the different SLRs within
936 pollution layers. Data are separated based on the different air mass origin (Western Sector, Eastern
937 Sector, and Open Sea).
938

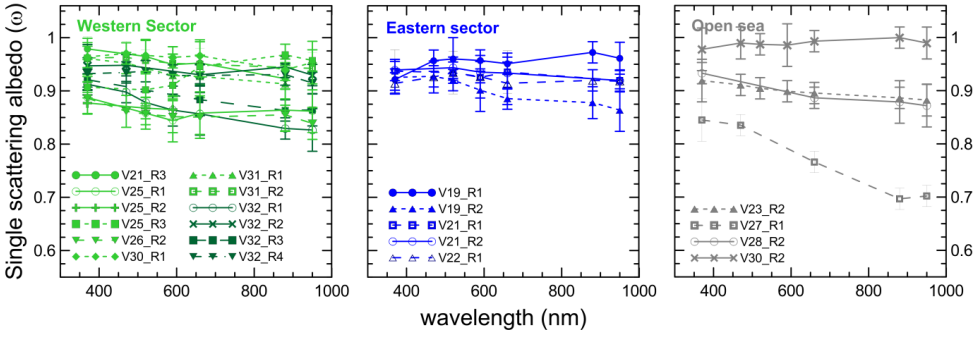

939
940
941

Atmos. Chem. Phys. Discuss., doi:10.5194/acp-2016-47, 2016
Manuscript under review for journal Atmos. Chem. Phys.
Published: 11 April 2016

Atmospheric Chemistry and Physics Discussions

942 **Figure 5.** Single scattering albedo (370, 660, and 950 nm), ozone enhancement factor ($\Delta O_3/\Delta CO$),
943 Aitken-to-accumulation ratio (dN_{Aitken}/dN_{Acc}), and scattering (SAE) and absorption Ångström
944 exponent (AAE) versus height for all analysed SLRs cases.
945

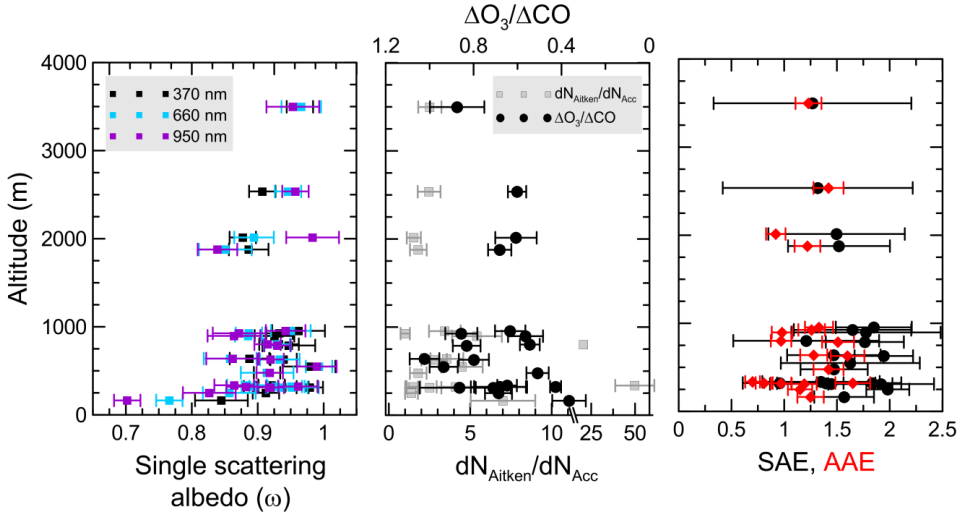

946
947
948

949 **Figure 6.** Comparison of the aerosol scattering (σ_s, left panel) and absorption (σ_{abs}, right panel)
950 coefficients measured by the nephelometer and the aethalometer and calculated from measured size
951 distribution data with Mie theory. Data are given at ambient conditions.
952

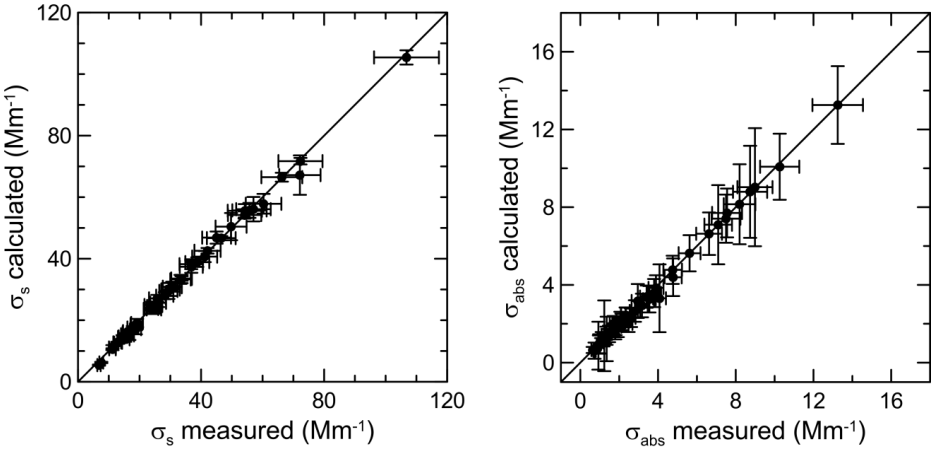

953
954

Atmos. Chem. Phys. Discuss., doi:10.5194/acp-2016-47, 2016
Manuscript under review for journal Atmos. Chem. Phys.
Published: 11 April 2016

Atmospheric Chemistry and Physics Discussions

Figure 7. Spectral real (n, left panel) and imaginary (k, right panel) parts of the complex refractive index obtained by optical closure for the 8 selected case studies. For sake of clarity, uncertainties on n and k are not reported in the plot. The values of the single scattering albedo measured at 370 and 950 nm for the different cases are reported in the legend. The spectral real and imaginary parts of the complex refractive index as obtained from the Optical Properties of Aerosols and Clouds (OPAC, Hess et al., 1998) database for insoluble, water soluble, soot and sea salt components are also reported in the plot. These components are used in OPAC to model continental polluted, continental rural, urban, and maritime polluted aerosols.

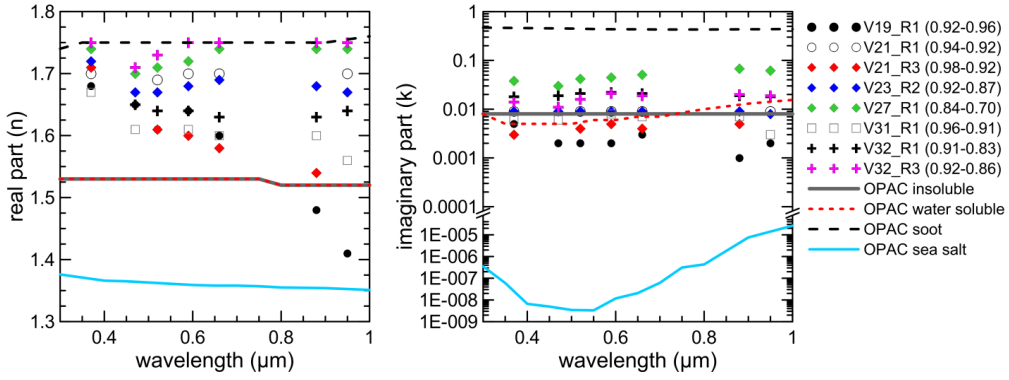

Figure 8. Spectral single scattering albedo plotted against the real (left panel) and the imaginary (right panel) parts of the complex refractive index.

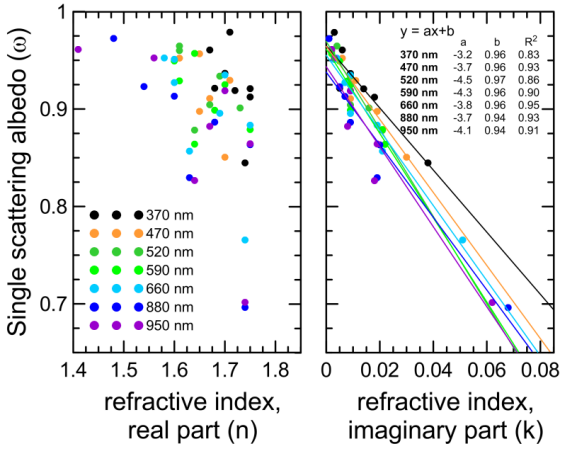

Atmos. Chem. Phys. Discuss., doi:10.5194/acp-2016-47, 2016
Manuscript under review for journal Atmos. Chem. Phys.
Published: 11 April 2016

Atmospheric Chemistry and Physics Discussions

970 **Figure 9.** Aerosol shortwave forcing efficiency at 60° solar zenith angle calculated at the surface,
971 TOA, and within the atmosphere for the maximum, mean, and minimum of the single scattering
972 albedo (ω) observed in this study (Table 4).
973

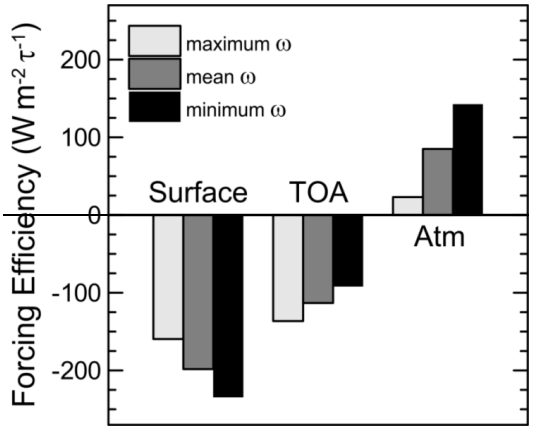

974